AGU PUBLICATIONS

JGR

Journal of Geophysical Research: Atmospheres

RESEARCH ARTICLE
10.1002/2015JD024167

Key Points:
- An ensemble approach of 3DCVA is introduced
- The derived forcing data are sensitive to background data and precipitation
- The uncertainties in forcing data can be used to evaluate model biases

Correspondence to:
S. Tang,
tang32@llnl.gov

Citation:
Tang, S., M. Zhang, and S. Xie (2016), An ensemble constrained variational analysis of atmospheric forcing data and its application to evaluate clouds in CAM5, *J. Geophys. Res. Atmos.*, *121*, 33–48, doi:10.1002/2015JD024167.

Received 1 SEP 2015
Accepted 1 DEC 2015
Accepted article online 5 DEC 2015
Published online 5 JAN 2016

An ensemble constrained variational analysis of atmospheric forcing data and its application to evaluate clouds in CAM5

Shuaiqi Tang[1,2], Minghua Zhang[1], and Shaocheng Xie[2]

[1]School of Marine and Atmospheric Sciences, Stony Brook University, Stony Brook, New York, USA, [2]Lawrence Livermore National Laboratory, Livermore, California, USA

Abstract Large-scale atmospheric forcing data can greatly impact the simulations of atmospheric process models (e.g., large eddy simulations, cloud-resolving models, and single column models (SCMs)) that are used to develop physical parameterizations in global climate models. This study introduces an ensemble variationally constrained objective analysis of atmospheric large-scale forcing data and its application to evaluate the cloud biases in the Community Atmospheric Model (CAM5). Sensitivities of the variational objective analysis to background data, error covariance matrix, and constraint variables are presented to quantify the uncertainties in the large-scale forcing data and state variables. Application of the ensemble forcing in the CAM5 SCM during March 2000 intensive operational period at the Southern Great Plains (SGP) of the Atmospheric Radiation Measurement Program shows that the systematic biases in the model simulations (i.e., excessive high clouds and insufficient low clouds) cannot be explained by the uncertainty of large-scale forcing data, which points to the deficiencies of physical parameterizations. These biases are found to also exist in the global simulation of CAM5 when it is compared with satellite data over the surrounding SGP site for annual and seasonal means.

1. Introduction

Clouds represent one of the largest uncertainties in current general circulation models (GCMs) simulations. Cloud simulations are found to have large discrepancies from satellite- and ground-based observations. *Zhang et al*. [2005] found that the majority of 10 GCMs only simulated 30% to 40% of the observed middle clouds and half of them underestimate low clouds comparing to satellite cloud analysis from International Satellite Cloud Climatology Project and CERES (Cloud and the Earth's Radiant Energy System). *Xie et al*. [2005] evaluated nine single column models (SCMs) and four cloud-resolving models (CRMs) using Atmospheric Radiation Measurement (ARM) Baseline Microphysical Retrieval (MICROBASE) ground measurements for a midlatitude cyclone system and found that the models generally captured the bulk characteristics of frontal clouds but differed significantly in the detailed structures. *Klein et al*. [2009] compared the simulations from 17 SCMs and 9 CRMs for an Arctic mixed-phase cloud case. They found that the median simulated liquid water path (LWP) is about one third of the observed value, and the spread among models are quite significant due to different physical schemes. *Jiang et al*. [2012] examined 19 CMIP5 (Coupled Model Intercomparison Project phase 5) models and found that both model observation difference and model spread are large especially at the upper troposphere levels. Some studies have attributed the model discrepancies to cloud parameterization errors other than to large-scale errors [e.g., *Su et al*., 2013]; however, it is still unclear how the physical parameterization and the large-scale atmospheric circulation each contribute to the model errors. Moreover, the uncertainties of cloud retrievals from different measurements and different retrieval algorithms are also large enough to affect the evaluation of model results [*Huang et al*., 2012; *Zhao et al*., 2012].

With the uncertainty of large-scale dynamics specified, we can better attribute the source of model biases. The large-scale forcing data (including vertical velocities and advective tendencies) are needed to drive the physics in large eddy simulations (LES) [e.g., *Khairoutdinov and Kogan*, 2000; *Zhang et al*., 2012], CRMs [e.g., *Khairoutdinov and Randall*, 2003; *Xu and Randall*, 1996; *Xu et al*., 2002], and SCMs [e.g., *Del Genio et al*., 2005; *Randall et al*., 1996; *Xie et al*., 2002, 2005] which are important tools to develop and test physical parameterizations used in GCMs [*Randall et al*., 1996] such as convections, turbulence, cloud microphysics, and macrophysics. To compare LES/CRM/SCM simulations with observations and to attribute model errors to deficiencies in physical parameterizations, accurate large-scale forcing data are needed.

Many objective analysis methods in the past have been carefully designed to derive large-scale forcing data from atmospheric sounding measurements [e.g., *Lin and Johnson*, 1996; *Ooyama*, 1987]. One widely used method is the constrained variational analysis algorithm (hereafter 1DCVA) developed by *Zhang and Lin* [1997]. Comparing to other conventional objective analysis methods, the unique feature of the 1DCVA makes use of surface and top of atmosphere (TOA) observations as constraints to adjust atmospheric state variables from sounding measurements. It makes the smallest possible amount of adjustments to conserve column-integrated mass, moisture, dry static energy, and momentum so that the final analysis data set is dynamically and thermodynamically consistent. This method has been used in the ARM program and several other field campaigns [e.g., *Schumacher et al*., 2007, 2008; *Xie et al*., 2005, 2006, 2010a]. Recently, *Tang and Zhang* [2015] extended the 1DCVA algorithm into a three-dimensional Constrained Variational Analysis (hereafter 3DCVA) at higher horizontal resolution and introduced additional features to improve the data quality. The new 3DCVA derives large-scale forcing data in each grid of a certain domain simultaneously, and all spatial grids interact with each other through advections.

Tang and Zhang [2015] recently proposed a 3DCVA approach. To reduce the large sensitivities of the forcing data to the input data, this paper introduces an ensemble approach of 3DCVA and quantifies the data uncertainties therein by analyzing the sensitivity of the forcing data to the background data of the atmospheric state variables, the specification of the error covariance matrix, and the constrained variables. As an application, the derived ensemble 3DCVA data are then used to evaluate the simulated clouds in the Community Atmospheric Model (CAM5) and diagnose the source of large biases in the model simulations. With the uncertainties of large-scale forcing quantified, the ensemble 3DCVA data allow us to more confidently attribute errors in the LES/CRM/SCM to physical sources when their simulated results are compared with observations.

The paper is organized as follows. Section 2 describes the method of ensemble 3DCVA and data used in the method. Section 3 shows the ensemble mean features of large-scale forcing data for one selected case and the sensitivities due to different background data, error covariance matrix, and constraint variables. Section 4 shows the sensitivities of SCM simulations due to large-scale forcing data and provides an example of cloud bias evaluation and error source diagnosis. Summary and discussion are given in section 5.

2. Method and Data of Ensemble 3DCVA

As described in *Tang and Zhang* [2015], the 3DCVA follows the general idea of 1DCVA [*Zhang and Lin*, 1997] that the atmospheric state variables (referred to as background data hereafter) u, v, q, and s are adjusted to minimize the cost function:

$$I = (u-u_o)^T B_u^{-1}(u-u_o) + (v-v_o)^T B_v^{-1}(v-v_o) + (q-q_o) + (s-s_o)^T B_s^{-1}(s-s_o), \tag{1}$$

while maintaining the column-integrated conservation of mass, moisture, and energy simultaneously across all spatial grids in the analysis domain:

$$\left\langle \nabla\cdot\vec{V} \right\rangle = -\frac{1}{g}\frac{\mathrm{d}P_s}{\mathrm{d}t} \tag{2}$$

$$\frac{\partial\langle q\rangle}{\partial t} + \left\langle \nabla\cdot\vec{V}_q \right\rangle = E_s - P_{\mathrm{rec}} - \frac{\partial\langle q_l\rangle}{\partial t} \tag{3}$$

$$\frac{\partial\langle s\rangle}{\partial t} + \left\langle \nabla\cdot\vec{V}\,s \right\rangle = R_{\mathrm{TOA}} - R_{\mathrm{SFC}} + L_v P_{\mathrm{rec}} + SH + L_v\frac{\partial\langle q_l\rangle}{\partial t}. \tag{4}$$

In addition, it adds the extra radiative constraints:

$$\frac{\partial s}{\partial t} + \nabla\cdot\left(\vec{V}\,s\right) + \frac{\partial\omega s}{\partial p} = Q_{\mathrm{rad}} \tag{5}$$

at each level above observed cloud top (or a specified level when observed cloud top is low or absent) to physically reduce the spurious heating and cooling centers that are often seen near tropopause in both conventional objective analysis methods and 3DCVA. In the cost function equation (1), u, v, q, and s are column vectors of horizontal winds, water vapor mixing ratio, and dry static energy ($s = C_pT + gz$, where C_p is specific heat capacity of air at constant pressure) for all grids in each time step. The superscript T denotes the transpose of a vector, the subscript o denotes the initial state, and B represents error covariance matrix for each state variable. In the constraint equations (2)–(5), the bracket represents vertical integration from the

Table 1. Different Background Data, Error Covariance Matrix, and Constraint Variables Used in Ensemble 3DCVA

Sources of Uncertainties (Elements)	Ensemble Members Used for Each Elements
Background data	RUC, ERA-Interim, CFSR, JRA55, MERRA, NARR (for details see Table 2)
Error covariance matrix	Calculated from variance of time series, only auto correlation. Calculated from variance of ensemble members, only auto correlation. Calculated from variance of ensemble members, vertical correlation. Calculated from variance of ensemble members, horizontal correlation. Calculated from variance of ensemble members, horizontal and vertical correlation.
Constraint variables	Arkansas-Red Basin River Forecast Center (ABRFC) gridded precipitation products Upper bound: 1.4 × ABRFC precipitation amount Lower bound: 0.6 × ABRFC precipitation amount

surface to the top of atmosphere (TOA), E_s is surface evaporation, P_{rec} is surface precipitation, L_v is the latent heat of vaporization, q_l is cloud liquid water content, R_{TOA} and R_{SFC} are net downward radiation at TOA and at surface, SH is surface sensible heat flux, ω is vertical velocity in pressure coordinate, and Q_{rad} is radiative heating rate calculated by the Rapid Radiative Transfer Model for GCMs using the temperature and humidity profiles from the background data. Other variables are as commonly used in meteorology.

The details of 3DCVA are described in *Tang and Zhang* [2015]. Here we highlight three sources of uncertainties (referred to as elements hereafter) that impact the 3DCVA results: background data, error covariance matrix, and constraint variables. Background data are the first guess of the 3DCVA; all the adjustments are with respect to the original background data. Error covariance matrix, which is represented by B in equation (1), determines how the background data are adjusted spatially. Constraint variables, which are the right-hand side terms of the constraint equations (2)–(5), control the budget of the whole system. Previous studies [*Xie et al*., 2004; *Zhang et al*., 2001] have shown that precipitation is the dominant constraint variables during rainy periods. In this study, we run 3DCVA using different combinations from six background data, five error covariance matrices, and three precipitation estimates (Table 1, details described below) to analyze the uncertainties in the derived forcing fields.

The six background data are obtained from reanalysis/analysis products listed in Table 2. They are linearly interpolated into 0.5° × 0.5° horizontal resolution, 3-hourly time resolution and 27 vertical levels from 1000 hPa to 100 hPa. Most of the constraint variables are derived from ARM surface station measurements, which include the following data sets:

1. Surface Meteorological Observation Stations (SMOS) measuring precipitation, pressure, winds, temperature, and relative humidity at the surface.
2. Energy budget Bowen ratio (EBBR) stations measuring surface latent and sensible heat fluxes.
3. Oklahoma and Kansas mesonet stations (OKM and KAM) measuring surface precipitation, pressure, winds, and temperature.
4. Microwave radiometer (MWR) stations measuring the total cloud liquid water.

These surface measurements are interpolated into 0.5° × 0.5° horizontal resolution covering the SGP domain. If there are actual measurements within the 0.5° × 0.5° grid box, simple arithmetic averaging is used to obtain the value for that grid box. Under circumstances that multiple instruments observe the same quantities, their measurements are merged in the arithmetic averaging process with a weighting function depending on their

Table 2. The Six Background Data Used in the Ensemble 3DCVA[a]

Name	Data Assimilation	Assimilation Intervals	Model Resolution	Model Vertical Levels
ERA-Interim [*Dee et al*., 2011]	4DVAR	12 h	T255 (79 km × 79 km)	60
CFSR [*Saha et al*., 2010]	3DVAR with flow dependence error variance	6 h	T382 (38 km × 38 km)	64
MERRA [*Rienecker et al*., 2011]	3DVAR with incremental analysis update	6 h	1/2° × 2/3°	72
JRA55 [*Kobayashi et al*., 2015]	4DVAR	6 h	TL319 (55 km × 55 km)	60
NARR [*Mesinger et al*., 2006]	3DVAR with precipitation assimilated	3 h	32 km × 32 km	45
RUC [*Benjamin et al*., 2004]	3DVAR	1 h	40 km × 40 km	40

[a]All data sets are interpolated into 0.5° × 0.5° horizontal resolution, 27 vertical levels from 1000 hPa to 100 hPa, and 3-hourly time resolution.

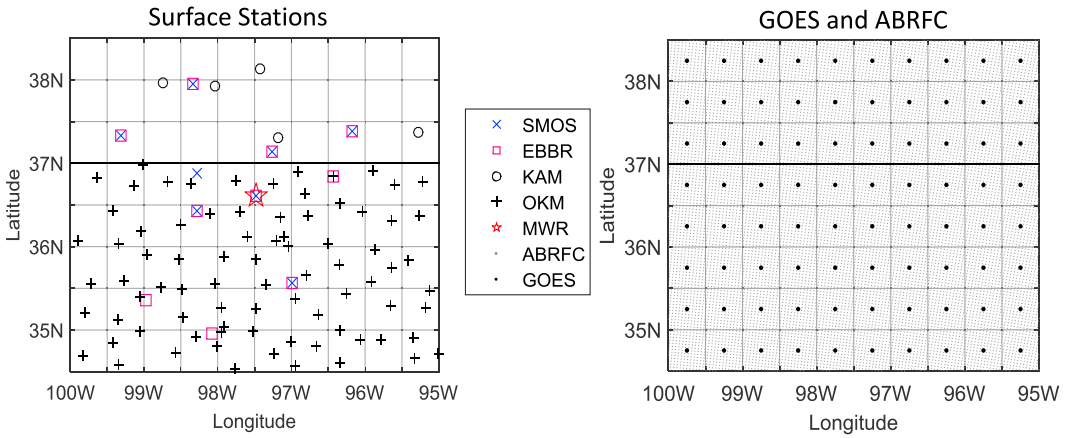

Figure 1. (left) Surface stations and (right) GOES TOA measurements and ABRFC gridded precipitation data. Different marks show different instruments. Gray lines show 0.5° × 0.5° grids in 3DCVA which are the same as grids of GOES satellite products (black dots). Black line at 37°N indicates the boundary between Oklahoma (below) and Kansas (above).

quality. If there is no actual measurement in the grid box, the Barnes scheme [*Barnes*, 1964] is used with the length scale of $L_x = 50$ km, $L_y = 50$ km, and $L_t = 6$ h to fill the missing grid box. The satellite measurements of radiative fluxes and cloud top pressure are available at NASA Langley Research Center [*Minnis et al*., 2008] measured by the Geostationary Operational Environment Satellite 8 (GOES8) in 0.5° × 0.5° grid box. The precipitation rate data are obtained from the 4 km resolution gridded precipitation products from Arkansas-Red Basin River Forecast Center (ABRFC) based on WSD-88 rain radar and gauge measurements and are averaged into 0.5° × 0.5° horizontal resolution and 3-hourly time resolution. Stational precipitation measurements from SMOS, OKM, and KAM are only used to fill the missing gap of ABRFC precipitation. The spatial distributions of the surface and TOA measurements used in this study are shown in Figure 1.

Surface and TOA measurements of constraint variables contain errors from instrument uncertainties, assumptions and limitations in the retrieval algorithms, and interpolation from stations to regular grids. As shown in *Zhang et al*. [2001] and *Xie et al*. [2004], precipitation is the most dominant constraint during precipitation periods. In this study, we will focus on the impact of precipitation uncertainties on the derived large-scale forcing data. Following *Xie et al*. [2014], we consider a 40% fractional root-mean-square error for ABRFC rainfall products, and use the estimated rain rate, the upper bound (1.4 times estimated rain rate), and the lower bound (0.6 times estimated rain rate) of the uncertainty to form the ensemble members. The 40% uncertainty is only considered on the magnitude of the rain rate.

We have two methods to calculate the error covariance matrix. One method is the original algorithm [*Zhang and Lin*, 1997; *Zhang et al*., 2001] in 1DCVA, which calculates the covariance from the variance of time series of the background data plus instrument and measurement uncertainties with no correlation. The other method is described in *Tang and Zhang* [2015] which calculates the covariance by using the anomaly of different background data relative to their ensemble mean. In this method, we can have the different correlation types of no correlation, vertical correlation only, horizontal correlation only, and both horizontal and vertical correlations in which adjustments of each grid point will have different correlations to its surrounding grids and levels. In total we can have five error covariance matrices to run the ensemble 3DCVA. Combining six background fields, three precipitation rates (representing constraint variables), and five covariance matrices, we therefore have a total of 90 3DCVA ensemble members.

An SCM version of CAM5 (SCAM5) is used to test the impact of uncertainties in the large-scale forcing data. CAM5 is the latest version of the NSF/Department of Energy (DOE) Community Atmospheric Model developed at the Nation Center for Atmospheric Research (NCAR), which contains a range of significant enhancements in the representation of moist physical processes relative to its predecessors [*Neale et al*., 2012]. These include (1) a turbulent kinetic energy based boundary layer scheme that can explicitly simulate stratus-radiation-boundary layer interactions [*Bretherton and Park*, 2009], (2) a new shallow convection scheme combined with the above boundary layer scheme [*Park and Bretherton*, 2009], and (3) a new bulk two-moment cloud microphysics scheme for stratiform clouds [*Morrison and Gettelman*, 2008] that predicts

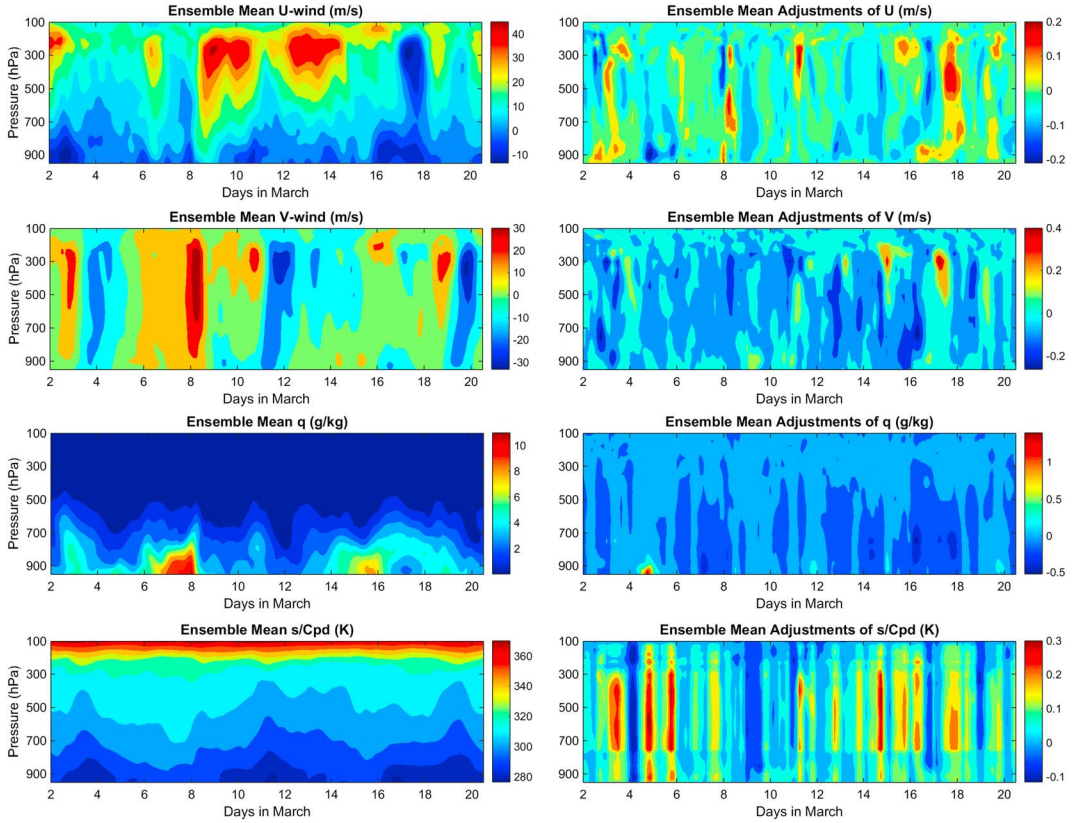

Figure 2. (left column) SGP domain averaged ensemble mean horizontal winds, moisture, and dry static energy (*u*, *v*, *q*, and *s*) and (right column) SGP domain averaged adjustments of *u*, *v*, *q*, and *s*.

both mixing ratios and number concentrations of cloud droplets (liquid) and crystals (ice). CAM5 is part of the Community Earth System Model that has been used in phase 5 of the Coupled Model Intercomparison Project (CMIP5).

The observed cloud properties used to evaluate the SCAM5 simulations are obtained from ARM Baseline Microphysical Retrieval (MICROBASE) which is a cloud retrieval product combining multiple measurements from cloud radar, lidar, ceilometer, microwave radiometer, and soundings. Other variables such as liquid water path (LWP) and radiative fluxes are obtained from ARM Best Estimate (ARMBE) products [*Xie et al.*, 2010b] at SGP central facility. We average these data into 3 h intervals in order to compare with SCAM5 simulations.

The satellite retrievals used to evaluate the CAM5 GCM results is the merged CALIPSO, CloudSat, CERES, and Moderate Resolution Imaging Spectroradiometer (MODIS) product C3M [*Kato et al.*, 2011]. It has global coverage from July 2006 to June 2010 for 4 years. Cloud fraction in this product is obtained from the percentage of cloudy CALIPSO bins within each analysis layer in all valid profiles. CloudSat clouds are assigned into CALIPSO bins. Liquid water content (LWC) and ice water content (IWC) are derived from the radar-only algorithm from CloudSat and normalized by LWP from MODIS retrievals. These profiles are projected to CERES footprint (20 km) and then averaged into $2° \times 2.5°$ horizontal resolution.

3. Ensemble Constrained Variational Analysis of Large-Scale Forcing Data

3.1. Ensemble Mean

The ARM March 2000 Intensive Operational Period (IOP) at the Southern Great Plains (SGP) is analyzed in this study. This IOP contains several precipitation events with various types of clouds, which has been extensively examined in earlier process studies [e.g., *Xie et al.*, 2005; *Xu et al.*, 2005]. The 3-D structure of a midlatitude cyclone case on 3 March has been analyzed by *Tang and Zhang* [2015]. Here we emphasize the SGP domain averaged large-scale forcing data during the whole IOP. The horizontal variabilities and sensitivities to the

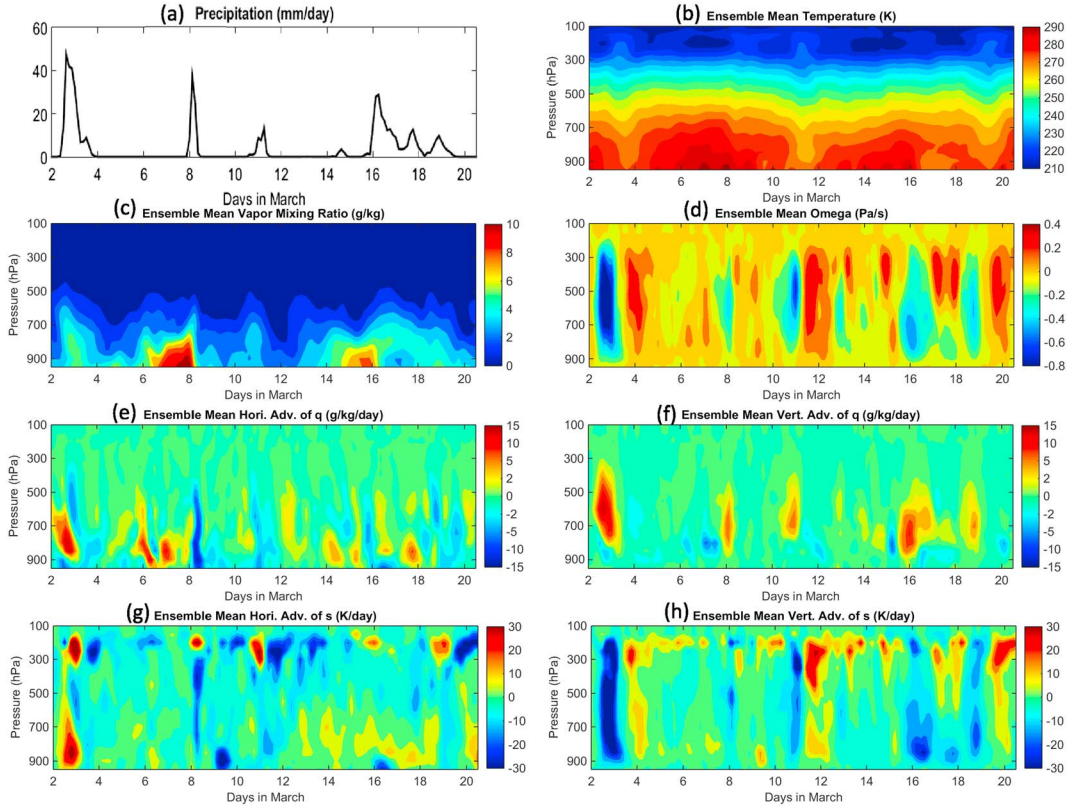

Figure 3. (a) SGP domain averaged precipitation and domain averaged ensemble mean profiles of (b) temperature, (c) water vapor mixing ratio, (d) vertical velocity, and (e–h) horizontal and vertical advections of q and s.

horizontal resolution will be investigated in a follow-up paper. The SGP domain in this study is following the domain used in *Tang and Zhang* [2015], which is a rectangle domain from 34.5–39°N, 95–100°W, with $0.5° \times 0.5°$ horizontal resolution shown in Figure 1.

Figure 2 shows the domain averaged ensemble mean analyzed u, v, q, and s from the ensemble 3DCVA, and the domain averaged ensemble mean adjustments for each variable. The domain mean adjustments of horizontal winds are smaller than $0.5\,\mathrm{m\,s^{-1}}$, but the standard deviation of adjustments on horizontal grids (not shown) are in the magnitude of $1\,\mathrm{m\,s^{-1}}$, indicating that the winds adjustments have compensatory effects horizontally, which brings large change to the divergence and advections. The average adjustment of q is generally smaller than $0.5\,\mathrm{g\,kg^{-1}}$, except for one low-level point at 18 Z on 4 March. Adjustments of s have a diurnal cycle with warm adjustments of ~0.3 K in the daytime and cold adjustments of ~0.1 K in the nighttime. The periodic feature of s adjustments indicates that the diurnal cycle of the background analysis data and the column energy budget is inconsistent. The sharp gradients of s adjustments at ~750 hPa and ~250 hPa may be due to the sharp change of vertical resolution from 25 hPa at lower and upper atmosphere to 50 hPa at middle troposphere (which is the typical vertical resolution settings in most global reanalysis data). We will use constant vertical resolution in future 3DCVA analysis. The domain averaged adjustment of q and s has a similar magnitude to the standard deviation of adjustments on horizontal grids (not shown).

Figure 3 shows the domain averaged precipitation and ensemble mean temperature, moisture, vertical velocity (omega), as well as horizontal and vertical advections of q and s, which are key variables of the large-scale state and forcing data. The precipitation occurs on 2–3 March, 8 March, 11 March, and 16–19 March, separately. The rising motion and advections of q and s correspond well with these events. The general patterns are also consistent with forcing data derived from 1DCVA (not shown), which use the same source of constraint variables within a slightly smaller domain at SGP. In the next section, we will discuss the impact of the three elements of ensemble 3DCVA on the analyzed state variables and large-scale forcing data.

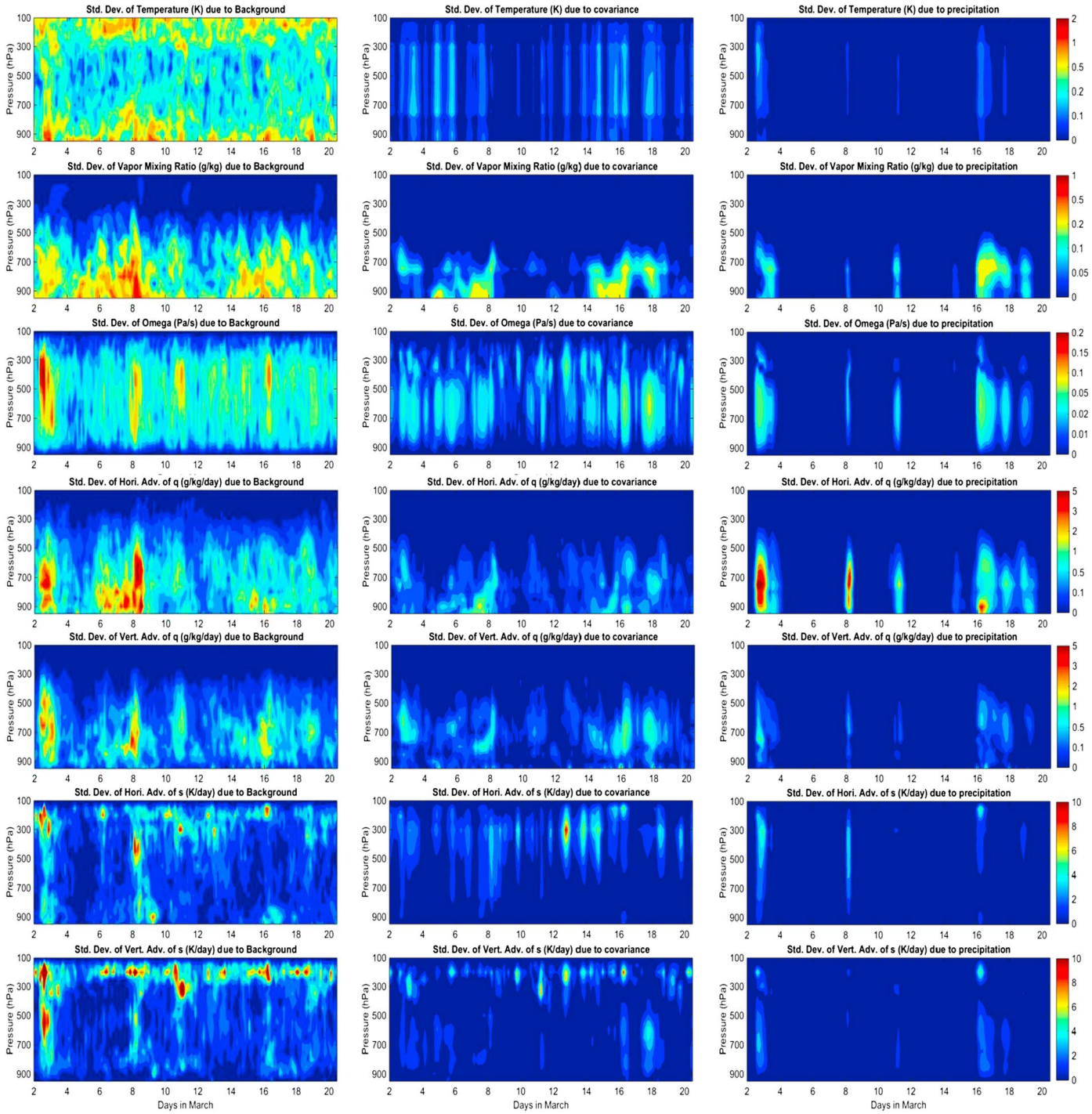

Figure 4. The standard deviations of state variables and large-scale forcing data (from top to bottom: T, q, ω, horizontal and vertical advections of q and s) to (left column) different background data, (middle column) error covariance matrices, and (right column) precipitation rates.

3.2. Analysis of Sensitivity and Uncertainty

To understand the sensitivities of atmospheric state variables and large-scale forcing data to different elements in 3DCVA, we calculated the standard deviations of them due to different background data, error covariance matrices, and precipitation rates (Figure 4). For a given element (such as background data), the averaged atmospheric state and forcing parameters are first calculated over all ensemble members of the other two elements (such as error covariance matrix and precipitation rate). The standard deviation is then computed over all

Table 3. The Vertically Averaged 1 Sigma Uncertainties of Atmospheric State Variables and Large-Scale Forcing Data Due To All Different Elements[a]

	Temperature	Water Vapor Mixing Ratio	Vertical Velocity	Advections of q	Advections of s
Whole IOP	1.5%	5.6%	21.6%	24.9%	27.0%
Precipitation	1.6%	6.3%	26.7%	32.5%	31.9%
Nonprecipitation	1.4%	4.9%	16.7%	17.6%	22.4%

[a]For advections of q and advections of s, the uncertainty is the average of the uncertainties of horizontal and vertical advections.

ensemble members of that one element. The magnitude of standard deviation of temperature and water vapor mixing ratio is generally smaller than 2 K and 1 g kg^{-1}, respectively; the magnitude of vertical velocity and advective tendencies of q and s are around 0.2 Pa s^{-1}, 5 g kg^{-1} d^{-1}, and 10 K d^{-1}, respectively. The relative uncertainties of vertical velocity and advective tendencies are much larger than the relative uncertainties of temperature and moisture. The standard deviation due to different background data is larger than that due to error covariance and precipitation in most of time, indicating the importance of the initial first guess to the final data. For uncertainties due to precipitation, horizontal moisture advection has much larger uncertainty than other variables, which indicates tight relationship between the horizontal moisture advection and precipitation process.

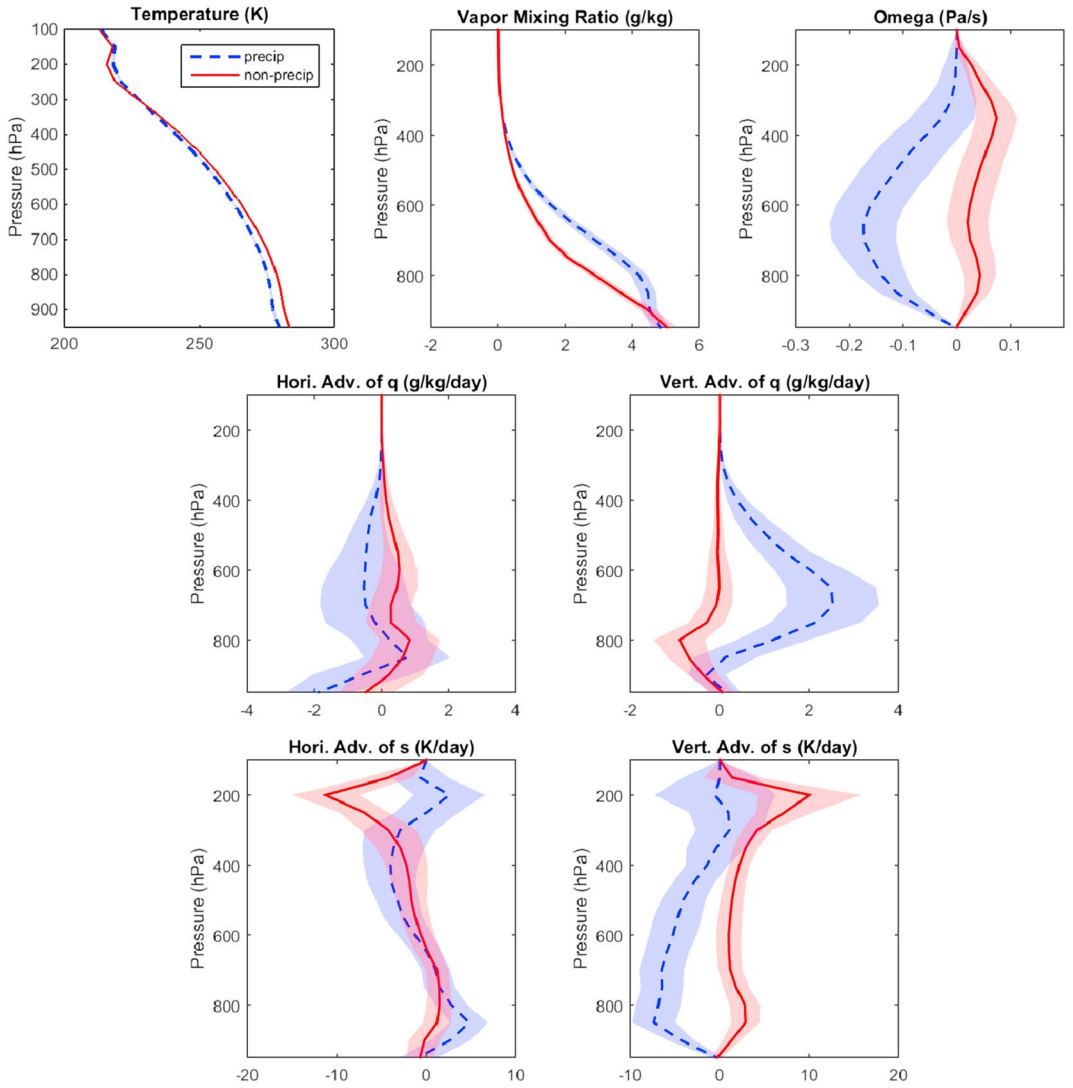

Figure 5. Ensemble mean vertical profiles of (top row) temperature, vapor mixing ratio, and vertical velocity; (middle row) horizontal and vertical advection of q; and (bottom row) horizontal and vertical advection of s averaged for precipitation period (blue) and nonprecipitation period (red). The time-mean standard deviations are shown as shaded areas.

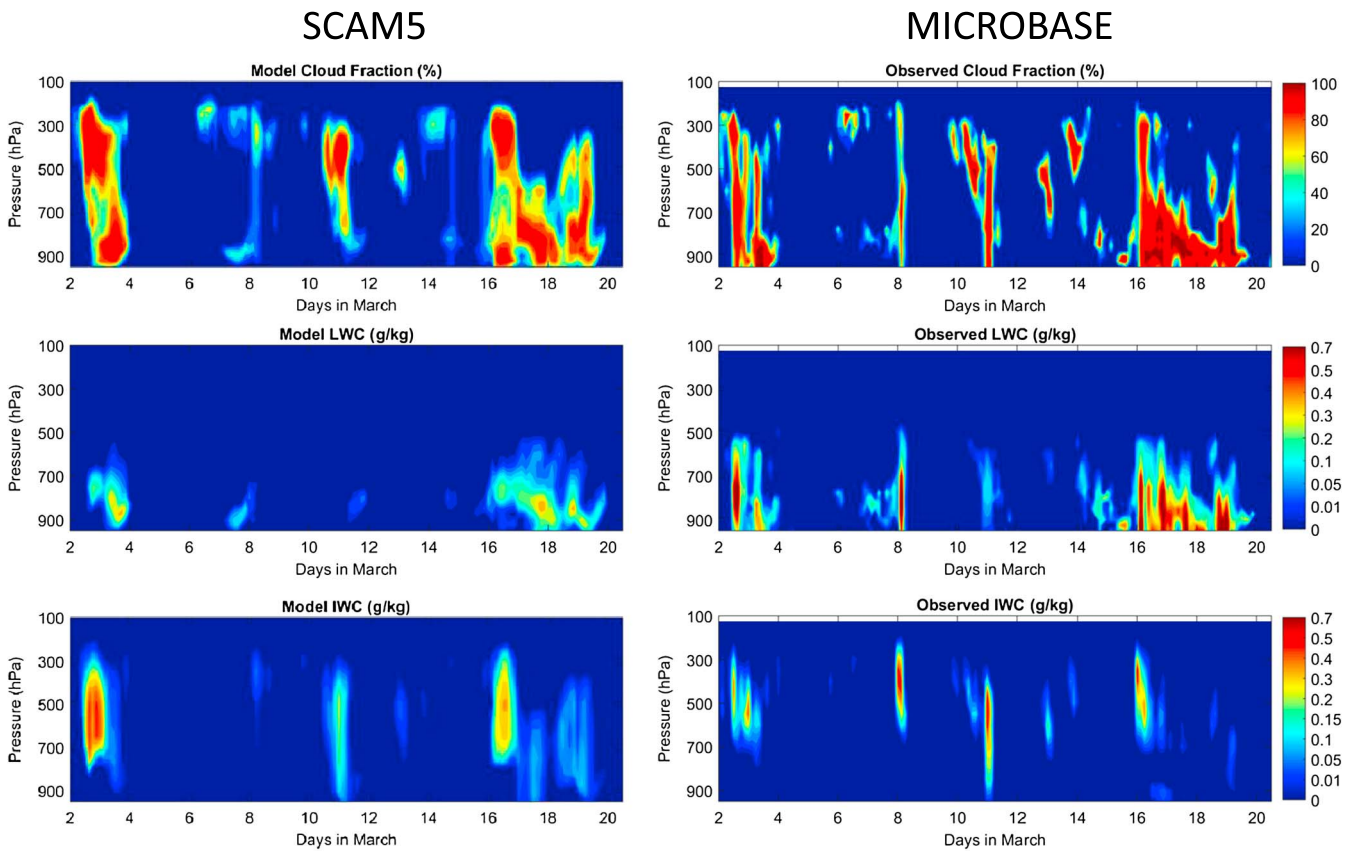

Figure 6. (left column) The ensemble average of SCAM5 simulated cloud properties and (right column) cloud retrievals from MICROBASE. From top to bottom: cloud fraction, LWC, and IWC (model IWC includes both cloud ice and snow).

To investigate the overall uncertainties of atmospheric state variables and large-scale forcing data due to all the three elements, we define the relative 1 sigma uncertainty as the standard deviation of the 90 ensemble members divided by the temporal standard deviation of the ensemble mean fields during the whole IOP. As shown in Table 3, during the whole IOP, the vertically averaged 1 sigma uncertainty is about 1.5% for temperature and 5.6% for vapor mixing ratio. If we separate it into precipitation periods and nonprecipitation periods (the denominator is still the temporal standard deviation during the whole IOP), the 1 sigma uncertainty in temperature (water vapor mixing ratio) is 1.6% (6.3%) for precipitation periods and 1.4% (4.9%) for nonprecipitation periods. For the analyzed forcing fields, the mean 1 sigma uncertainty in vertical velocity and advective tendencies of q and s is 21.6%, 24.9%, and 27.0% for the whole IOP, 26.7%, 32.5%, and 31.9% for precipitation periods, and 16.7%, 17.6%, and 22.4% for nonprecipitation periods, respectively. It is clear that these state variables and large-scale forcing data are more uncertain during precipitation periods than during nonprecipitation period.

The vertical profiles of these state variables and large-scale forcing data averaged over the precipitation period and nonprecipitation period and their standard deviations are shown in Figure 5. There are significant differences between vertical profiles of the precipitation period and nonprecipitation period. During the precipitation period, it has lower temperature and higher moisture at lower level. The vertical velocity shows ascent motion throughout the whole troposphere during the precipitation period, while descent motion during the nonprecipitation period, which contributes to opposite signs in vertical advections of q and s. Advections of s at upper levels have larger sensitivities than at middle and low levels, which may be related to the relatively larger gradient of s at the tropopause.

4. Application of Ensemble Forcing Data to Cloud Bias Evaluation

4.1. Sensitivity of SCM Simulations

We next analyze the sensitivity of SCM simulations to different elements of the ensemble 3DCVA in the large-scale forcing data. Here we run SCAM5 using each member of the ensemble large-scale forcing data (SGP

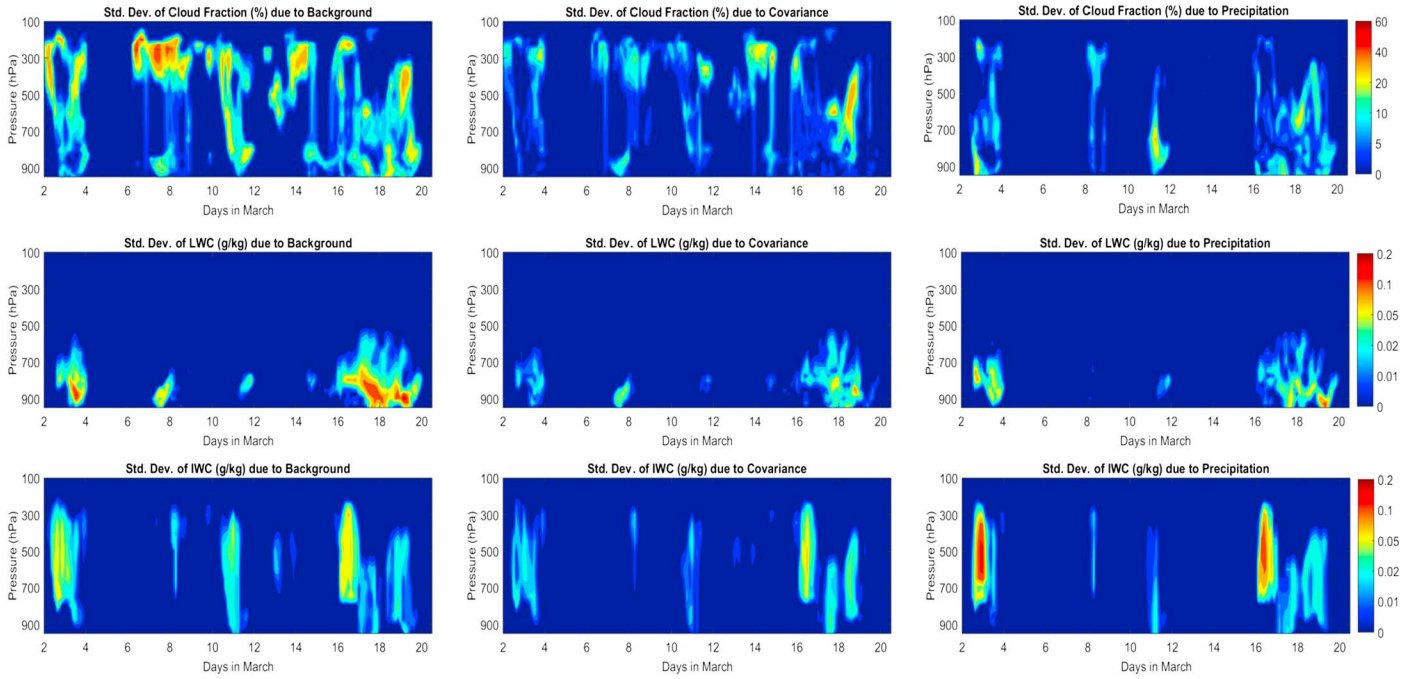

Figure 7. The standard deviations of SCAM5 simulated clouds (from top to bottom: cloud fraction, LWC, and IWC) due to (left column) different background data, (middle column) error covariance matrices, and (right column) precipitation.

domain mean), restarting at 15 Z every day from 1 March to 19 March for 36 h without relaxation, and choose the hour 9 to 33 of the simulations (00 Z to 24 Z of the next day) to test the sensitivities of model results to different background data, error covariance matrices, and constraint variables. Surface sensible and latent heat fluxes are prescribed from the constraint variables.

The time-pressure cross sections of the ensemble mean simulated cloud fraction, liquid water content (LWC), and ice water content (IWC) are shown in Figure 6 (left column). Also shown in the figure are the observations obtained from MICROBASE during this period (Figure 6, right column). Note that the modeled IWC in this study includes both cloud ice and snow since observation does not separate the two. The model captured most of the major cloud events during the IOP, with good consistency to observations especially in the cloud fraction.

The standard deviations of simulated cloud fraction, LWC, and IWC to different elements of the ensemble 3DCVA are shown in Figure 7. The uncertainty of cloud properties at some time steps could reach up to more than 50% of simulated values, showing that the amount of cloud fraction and hydrometeors are quite sensitive to the large-scale forcing data. The mean 1 sigma uncertainty is about 25.9% for cloud fraction, 17.6% for LWC, and 16.1% for IWC. Among the three elements in 3DCVA, background data are the largest contributor to uncertainties of cloud fraction and LWC, which is similar to the results of the large-scale forcing data in the previous section. However, IWC is more sensitive to the precipitation rather than to the background data. Further analysis shows that the cloud ice is more sensitive to the background data, but snow, which is much larger than cloud ice mixing ratio, is more sensitive to the precipitation. Overall, different elements in the 3DCVA have considerable impacts on SCM cloud simulation.

4.2. Evaluation of Model Biases Using Ensemble Simulations

In SCMs, model errors come from two sources: deficiencies in physical parameterizations and uncertainties in large-scale forcing data. By considering uncertainties in both large-scale forcing data and observed validation data, we can better identify the source of model bias (discrepancy between models and observations): whether the model bias can be explained by the uncertainties in forcing data and observed validation data or if it comes from physical parameterizations.

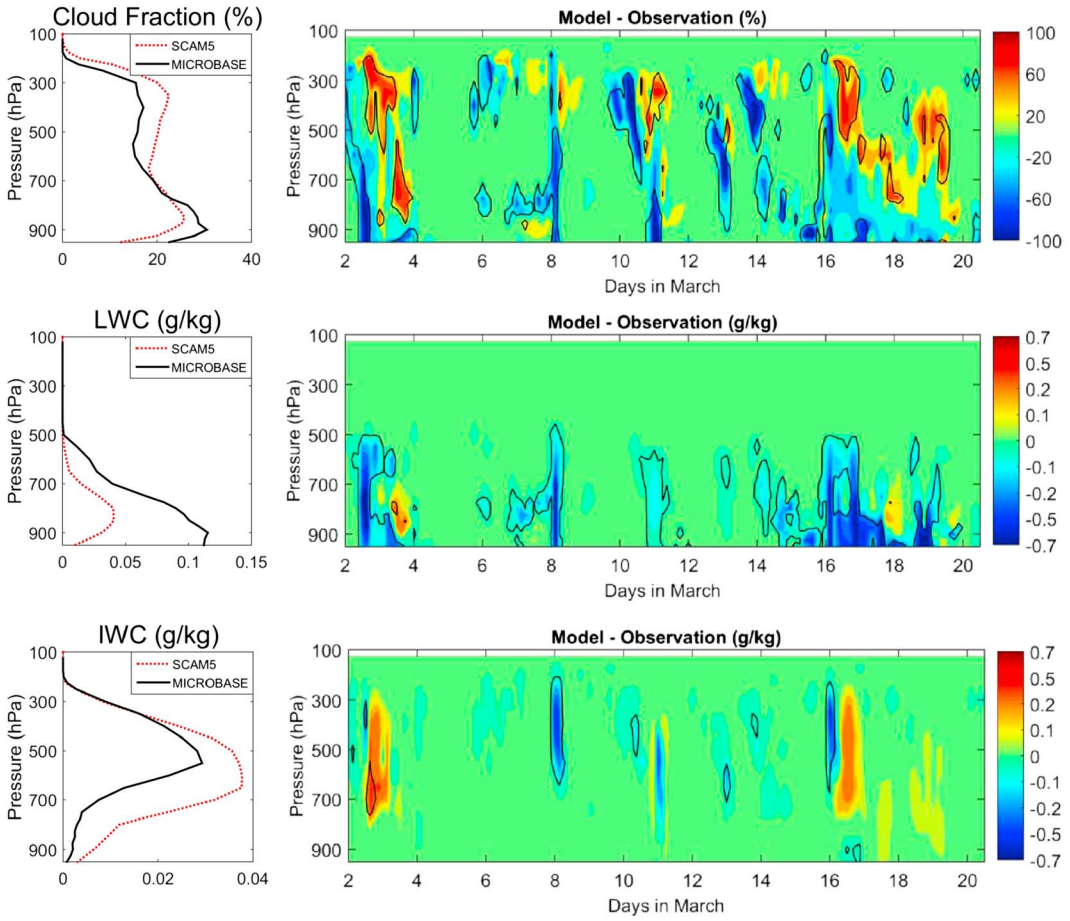

Figure 8. (right column) SCAM5 model bias of cloud properties. Blue color means model underestimation while yellow/red means overestimation, with black lines circle out where model bias is larger than the total uncertainties from large-scale forcing data and observations. (left column) Vertical profiles averaged during the whole period. Black line is MICROBASE; red dashed line is SCAM5. From top to bottom: cloud fraction, LWC, and IWC (IWC includes both cloud ice and snow).

In this study, the model uncertainties due to large-scale forcing data are estimated as twice of the model standard deviation (2 sigma uncertainty, which equals to about 95% uncertainty assuming Gaussian distribution) using different large-scale forcing data from all 90 3DCVA members listed in Table 1. The uncertainties in the MICROBASE cloud retrievals are estimated as 15% for LWC, 55% for IWC, and 25% for cloud fraction. These numbers are based on the study by *Zhao et al.* [2014] in which they perturbed key inputs and parameters in cloud retrieval algorithms and estimated these uncertainties. Limitations and caveats about the cloud retrievals will be discussed later.

Figure 8 shows the model bias of cloud fraction, LWC, and IWC in time-pressure profiles (right), and the vertical profiles averaged in the whole period (left). The black lines in the right panel highlight regions where model biases are larger than the uncertainties from forcing data and observations:

$$|\mathrm{SCAM5} - \mathrm{MICROBASE}| > \sqrt{\left(2\sigma_{\mathrm{forcing}}\right)^2 + \sigma_{\mathrm{obs}}^2}, \tag{6}$$

where $\sigma_{\mathrm{forcing}}$ is the 1 sigma uncertainty of SCAM5 simulations due to different forcing data, and σ_{obs} is the observation uncertainty specified above. It is seen that SCAM5 overestimates high cloud, while underestimates low cloud, consistent with its overestimation of IWC and underestimation of LWC. Most of these biases are significantly larger than the total uncertainties from large-scale forcing data and observations, indicating that these biases are due to the deficiencies of physical parameterizations in the model. For IWC, most of the model overestimation is within the uncertainties from large-scale forcing data and observations.

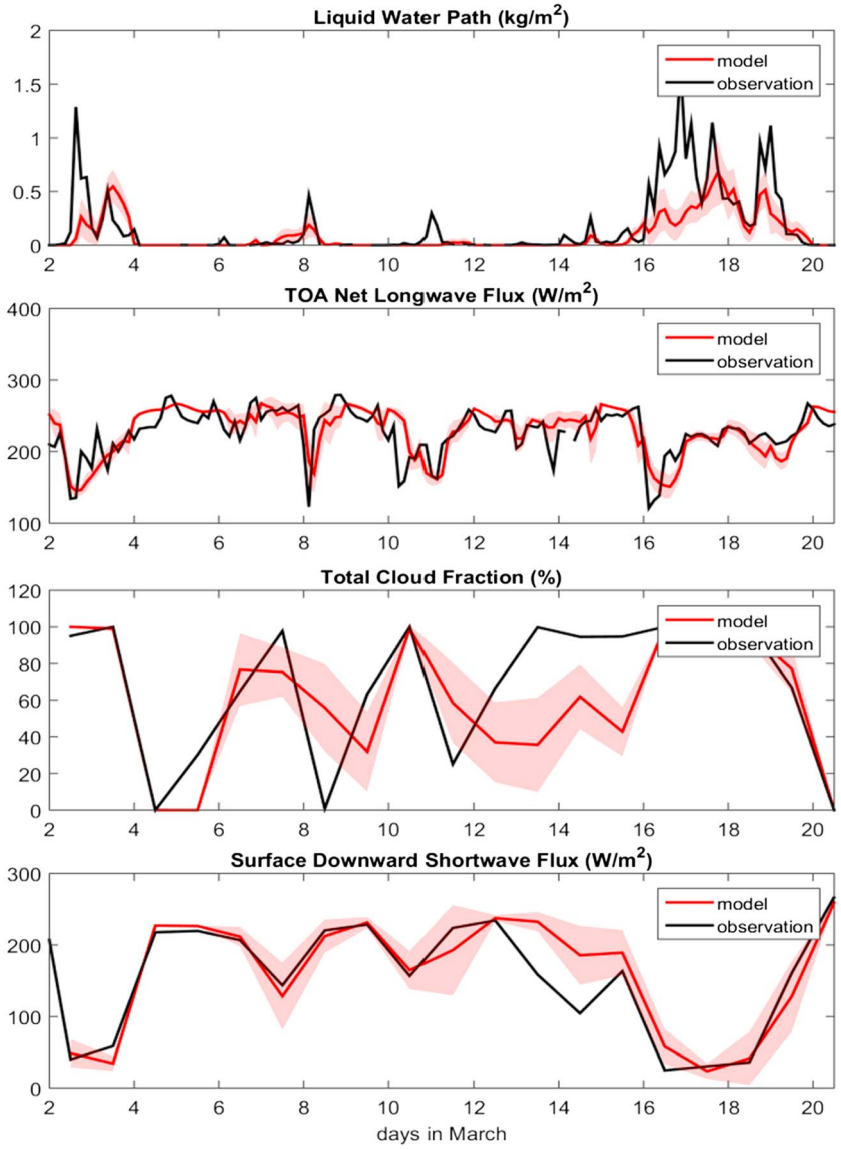

Figure 9. Ensemble mean SCAM5 simulations (red line) with standard deviations due to different large-scale forcing data (red shade) and observations from ARMBE (black). From top to bottom: LWP, TOA net longwave flux, total cloud fraction (daytime mean), and surface downward shortwave flux (daily mean).

The uncertainties of the cloud hydrometeor retrievals given above could be underestimated. *Zhao et al*. [2014] pointed out that when considering all assumptions and for precipitating clouds, uncertainties could be larger than those given in this study. The spread among different retrieval products may be much larger than the diagnosed uncertainties [*Zhao et al*., 2012]. Later analysis will also show this large spread (Figure 10). *Huang et al*. [2012] suggests that different input data, different treatments of rain contamination, and mixed-phase clouds are mainly responsible for the large differences of retrieved LWC.

Given the large uncertainties in the cloud retrievals, it is important to examine if model errors shown in cloud properties are consistent with those exhibited in other relevant fields. Figure 9 compares the LWP, outgoing longwave flux at TOA, total cloud fraction (daytime mean), and surface downward shortwave flux (daily mean) between the observations (ARMBE) and SCAM5 simulations. The standard deviations of model simulations due to different forcing data are shown in the shaded area. The use of daily averaging for the surface downward shortwave flux is to remove the strong diurnal cycle and the use of daytime averaging for the total

cloud fraction is to make it consistent with surface downward shortwave flux because there is no shortwave flux at nighttime. The time variations of these variables are overall consistent with cloud fraction and hydrometeors during this period.

It can be seen that the LWP in SCAM5 is lower than the observed value during most of cloud/precipitation events. The simulated LWP (with standard deviation, same as below) averaged during the whole IOP is $94.8 \pm 6.9\,g\,m^{-2}$, comparing to the observed $191.3\,g\,m^{-2}$. Note that LWC in MICROBASE has been constrained by the LWP at the SGP central facility so the LWC and LWP are not independent. We therefore examine the radiation fields at the TOA and surface, which are independent from the retrieved cloud properties.

For longwave flux at TOA, SCAM5 missed some cloud events on 10 and 14 March, where longwave flux has a sharp decrease in the observations but is relatively flat in the model. During the whole IOP, SCAM5 has TOA longwave flux of $229.4 \pm 1.1\,W\,m^{-2}$, slightly larger than the observed $227.6\,W\,m^{-2}$. However, the model does not always overestimate longwave flux at TOA. During times when SCAM5 has more high cloud fraction than observations in Figure 8, it also underestimates longwave flux (on 3, 17, and 19 March).

For total cloud fraction and surface downward shortwave flux, daily (daytime) averaging is used to smooth out some short-period cloud features. From 13 to 15 March, the model overestimation of surface downward shortwave fluxes is consistent with the underestimation of total cloud fraction. These consistencies between the biases of cloud properties with biases of radiation fluxes give us more confidence in attributing model biases to the deficiencies of physical parameterizations.

4.3. Applicability of SCM Results to GCM

The above analysis of model biases is limited to one single IOP. To understand the applicability of the SCM results in this IOP to the GCMs climatologically and globally, we compare the simulations of clouds in the CAM5 GCM with ARM MICROBASE data and satellite cloud retrievals C3M to examine if the biases in SCAM5 still exist in CAM5 GCM. The CAM5 GCM results are obtained from CAM5 Atmospheric Model Intercomparison Project run.

Figure 10 (top row) shows the climatological mean cloud fraction, LWC, and IWC at SGP site (or the nearest grid) from CAM5 (blue), C3M (red), and MICROBASE (black), respectively. Nine-point smoothing was applied on C3M and CAM5 to remove the noise. For cloud fraction, both the C3M and MICROBASE data show that CAM5 overestimates high clouds and underestimates low clouds, which is consistent with SCAM5 results discussed earlier. For LWC, the differences between the two observations are too large to draw a firm conclusion about the CAM5 GCM (note that the *x* axis is in logarithm scale). The reason of large LWC differences between C3M and MICROBASE remains unclear. One possible cause is the different assumptions used in the retrieval algorithms, where C3M assumes all clouds are liquid (ice) phase when retrieving LWC (IWC), while MICROBASE assumes cloud droplets number concentration is constant ($100\,cm^{-3}$). The cloud phase assumption may also lead to the large LWC at ~200 to 300 hPa in C3M. The CAM5 GCM is closer to the C3M profile than to the MICROBASE data below 400 hPa. However, this closer agreement might be accidental since CloudSat does not measure LWC well when there is a precipitation and C3M could underestimate LWC as well. For IWC, the differences among the two observations and model are relatively small.

Figure 10 (middle and bottom rows) shows cloud fraction, LWC, and IWC at SGP for June, July, and August (JJA) and December, January, and February (DJF), respectively. CAM5 overestimates high clouds, especially in JJA, while it underestimates low clouds, especially in DJF. C3M has an upper-level peak of LWC in both seasons and has IWC extending to the surface in summer, which may be caused by unrealistic assumptions in the retrieval algorithm.

Despite the large uncertainties in cloud retrievals of LWC and IWC, the model biases of the underestimation of low cloud fraction and overestimation of high cloud fraction in SCAM5 are confirmed to be systematic because the same biases also exist in CAM5 GCM. We see these biases in many other regions of the globe [e.g., *Cheng and Xu*, 2013; *Liu et al*., 2012; *Song et al*., 2012; *Xu and Cheng*, 2013a, 2013b] and for the global mean clouds (not shown). These global and climatological model biases in CAM5 GCM are overall consistent with SCM biases at SGP that were described before.

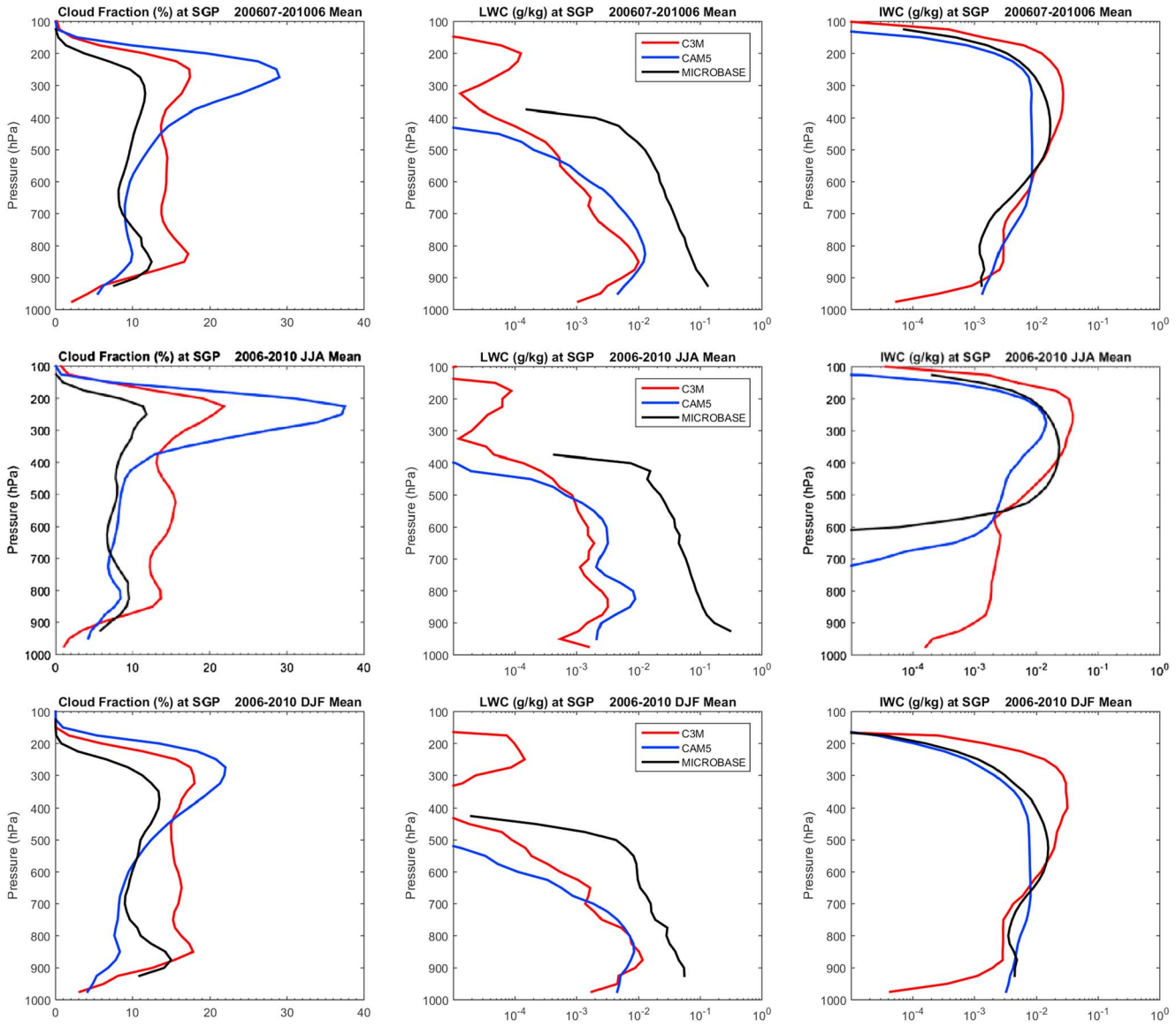

Figure 10. (top row) Four year (July 2006 to June 2010) mean, (middle row) JJA mean, and (bottom row) DJF mean profiles of (left column) cloud fraction, (middle column) LWC, and (right column) IWC at SGP site or the closest grid. Blue line is from CAM5 GCM; red line is from C3M merged satellite retrieval; black line is from MICROBASE ground retrieval. Nine-point smoothing is applied to C3M and CAM5 data to remove the noise.

5. Summary and Discussion

Background data, error covariance matrix, and constraint variables are three important sources of uncertainties (elements) in 3DCVA to derive the large-scale forcing data required by LES/CRM/SCM. We described an ensemble approach of 3DCVA using six sets of background data, five error covariance matrices, and three constraint variables (precipitation), in total 90 members. The ensemble approach quantifies the uncertainties of the atmospheric state variables and large-scale forcing data. The results show that all the three elements of the ensemble 3DCVA have considerable impact on the analyzed state variables and large-scale forcing data, especially to the vertical velocity and advective tendencies. Among the three elements, background data have the largest impact on the forcing data, while precipitation has relatively larger impact on the horizontal moisture advection.

With the uncertainty from the large-scale forcing data calculated and the uncertainty of observed clouds estimated, this study compared the simulated clouds in the SCAM5 with MICROBASE cloud retrievals. We

found that SCAM5 overestimates high clouds, while underestimates low clouds, and it underestimates LWC but overestimates IWC slightly. It also misses some cloud events. Most of these model biases are larger than the uncertainty from large-scale forcing data plus uncertainty from observations, indicating that these biases come from model parameterization deficiencies. These cloud biases are shown to be consistent with the model biases of surface and TOA radiative fluxes.

The applicability of the SCM results at the SGP in the March 2000 IOP to the global model is examined by comparing CAM5 GCM results with the C3M satellite retrievals at the grid point surrounding the SGP. We show consistent model biases in cloud fraction: CAM5 overestimates high clouds and underestimates low clouds. These results indicate that most of the GCM biases are caused by physical parameterizations rather than large-scale dynamics and that the SCM simulations forced by the ensemble large-scale forcing data can be used to further diagnose the cause of model errors in its physical parameterizations.

While the ensemble forcing provides a way to estimate the uncertainties in the large-scale forcing data, we point out that the specified uncertainties in the 3DCVA can be improved. This is especially true for the uncertainties in the input data of the constraint variables. The current method only uses uncertainties in the precipitation constraint that is scaled against the best estimate precipitation. More sophisticated specification requires knowledge of the spatial structure of the precipitation uncertainties as well as uncertainties in other constraint variables. With this caveat in mind, we believe the variationally constrained ensemble of large-scale forcing data described in this paper can be used to more confidently identify and quantify model errors from LES/CRM/SCM.

Acknowledgments

This research is supported by the Biological and Environmental Research Division in the Office of Sciences of the US Department of Energy (DOE), and by the National Science Foundation, to the Stony Brook University. Work at LLNL was supported by the DOE Atmospheric Radiation Measurement (ARM) program and performed under the auspices of the U. S. Department of Energy by Lawrence Livermore National Laboratory under contract DE-AC52-07NA27344. The 3DCVA source code and the data are available from the authors upon request (tang32@llnl.gov).

References

Barnes, S. L. (1964), A technique for maximizing details in numerical weather map analysis, *J. Appl. Meteorol.*, *3*(4), 396–409, doi:10.1175/1520-0450(1964)003<0396:ATFMDI>2.0.CO;2.

Benjamin, S. G., et al. (2004), An hourly assimilation–forecast cycle: The RUC, *Mon. Weather Rev.*, *132*(2), 495–518, doi:10.1175/1520-0493(2004)132<0495:AHACTR>2.0.CO;2.

Bretherton, C. S., and S. Park (2009), A new moist turbulence parameterization in the Community Atmosphere Model, *J. Clim.*, *22*(12), 3422–3448, doi:10.1175/2008JCLI2556.1.

Cheng, A., and K.-M. Xu (2013), Evaluating low-cloud simulation from an upgraded multiscale modeling framework model. Part III: Tropical and subtropical cloud transitions over the northern Pacific, *J. Clim.*, *26*(16), 5761–5781, doi:10.1175/JCLI-D-12-00650.1.

Dee, D. P., et al. (2011), The ERA-Interim reanalysis: Configuration and performance of the data assimilation system, *Q. J. R. Meteorol. Soc.*, *137*(656), 553–597, doi:10.1002/qj.828.

Del Genio, A. D., A. B. Wolf, and M.-S. Yao (2005), Evaluation of regional cloud feedbacks using single-column models, *J. Geophys. Res.*, *110* D15S13, doi:10.1029/2004JD005011.

Huang, D., C. Zhao, M. Dunn, X. Dong, G. G. Mace, M. P. Jensen, S. Xie, and Y. Liu (2012), An intercomparison of radar-based liquid cloud microphysics retrievals and implications for model evaluation studies, *Atmos. Meas. Tech.*, *5*(6), 1409–1424, doi:10.5194/amt-5-1409-2012.

Jiang, J. H., et al. (2012), Evaluation of cloud and water vapor simulations in CMIP5 climate models using NASA "A-Train" satellite observations, *J. Geophys. Res.*, *117*, D14105, doi:10.1029/2011JD017237.

Kato, S., et al. (2011), Improvements of top-of-atmosphere and surface irradiance computations with CALIPSO-, CloudSat-, and MODIS-derived cloud and aerosol properties, *J. Geophys. Res.*, *116*, D19209, doi:10.1029/2011JD016050.

Khairoutdinov, M., and Y. Kogan (2000), A new cloud physics parameterization in a large-eddy simulation model of marine stratocumulus, *Mon. Weather Rev.*, *128*(1), 229–243, doi:10.1175/1520-0493(2000)128<0229:ANCPPI>2.0.CO;2.

Khairoutdinov, M., and D. A. Randall (2003), Cloud resolving modeling of the ARM summer 1997 IOP: Model formulation, results, uncertainties, and sensitivities, *J. Atmos. Sci.*, *60*(4), 607–625, doi:10.1175/1520-0469(2003)060<0607:CRMOTA>2.0.CO;2.

Klein, S. A., et al. (2009), Intercomparison of model simulations of mixed-phase clouds observed during the ARM Mixed-Phase Arctic Cloud Experiment. I: Single-layer cloud, *Q. J. R. Meteorol. Soc.*, *135*(641), 979–1002, doi:10.1002/qj.416.

Kobayashi, S., et al. (2015), The JRA-55 reanalysis: General specifications and basic characteristics, *J. Meteorol. Soc. Jpn Ser. II*, *93*(1), 5–48, doi:10.2151/jmsj.2015-001.

Lin, X., and R. H. Johnson (1996), Kinematic and thermodynamic characteristics of the flow over the western Pacific warm pool during TOGA COARE, *J. Atmos. Sci.*, *53*(5), 695–715, doi:10.1175/1520-0469(1996)053<0695:KATCOT>2.0.CO;2.

Liu, X., X. Shi, K. Zhang, E. J. Jensen, A. Gettelman, D. Barahona, A. Nenes, and P. Lawson (2012), Sensitivity studies of dust ice nuclei effect on cirrus clouds with the Community Atmosphere Model CAM5, *Atmos. Chem. Phys.*, *12*(24), 12,061–12,079, doi:10.5194/acp-12-12061-2012.

Mesinger, F., et al. (2006), North American regional reanalysis, *Bull. Am. Meteorol. Soc.*, *87*(3), 343–360, doi:10.1175/bams-87-3-343.

Minnis, P., et al. (2008), Near-real time cloud retrievals from operational and research meteorological satellites paper presented at Proc. SPIE Europe Remote Sens, Cardiff, Wales, U. K., 15–18 Sept.

Morrison, H., and A. Gettelman (2008), A new two-moment bulk stratiform cloud microphysics scheme in the Community Atmosphere Model, version 3 (CAM3). Part I: Description and numerical tests, *J. Clim.*, *21*(15), 3642–3659, doi:10.1175/2008JCLI2105.1.

Neale, R. B., et al. (2012), Description of the NCAR Community Atmosphere Model (CAM 5.0) *NCAR Tech. Note Rep. NCARTN-4861STR*, 274 pp.

Ooyama, K. V. (1987), Scale-controlled objective analysis, *Mon. Weather Rev.*, *115*(10), 2479–2506, doi:10.1175/1520-0493(1987)115<2479:SCOA>2.0.CO;2.

Park, S., and C. S. Bretherton (2009), The University of Washington shallow convection and moist turbulence schemes and their impact on climate simulations with the Community Atmosphere Model, *J. Clim.*, *22*(12), 3449–3469, doi:10.1175/2008JCLI2557.1.

Randall, D. A., K.-M. Xu, R. J. C. Somerville, and S. Iacobellis (1996), Single-column models and cloud ensemble models as links between observations and climate models, *J. Clim.*, *9*(8), 1683–1697, doi:10.1175/1520-0442(1996)009<1683:SCMACE>2.0.CO;2.

Rienecker, M. M., et al. (2011), MERRA: NASA's modern-era retrospective analysis for research and applications, *J. Clim.*, *24*(14), 3624–3648, doi:10.1175/JCLI-D-11-00015.1.

Saha, S., et al. (2010), The NCEP climate forecast system reanalysis, *Bull. Am. Meteorol. Soc.*, *91*(8), 1015–1057, doi:10.1175/2010BAMS3001.1.

Schumacher, C., M. H. Zhang, and P. E. Ciesielski (2007), Heating structures of the TRMM field campaigns, *J. Atmos. Sci.*, *64*(7), 2593–2610, doi:10.1175/JAS3938.1.

Schumacher, C., P. E. Ciesielski, and M. H. Zhang (2008), Tropical cloud heating profiles: Analysis from KWAJEX, *Mon. Weather Rev.*, *136*(11), 4289–4300, doi:10.1175/2008MWR2275.1.

Song, X., G. J. Zhang, and J. L. F. Li (2012), Evaluation of microphysics parameterization for convective clouds in the NCAR Community Atmosphere Model CAM5, *J. Clim.*, *25*(24), 8568–8590, doi:10.1175/JCLI-D-11-00563.1.

Su, H., et al. (2013), Diagnosis of regime-dependent cloud simulation errors in CMIP5 models using "A-Train" satellite observations and reanalysis data, *J. Geophys. Res. Atmos.*, *118*, 2762–2780, doi:10.1029/2012JD018575.

Tang, S., and M. Zhang (2015), Three-dimensional constrained variational analysis: Approach and application to analysis of atmospheric diabatic heating and derivative fields during an ARM SGP intensive observational period, *J. Geophys. Res. Atmos.*, *120*, 7283–7299, doi:10.1002/2015JD023621.

Xie, S., et al. (2002), Intercomparison and evaluation of cumulus parametrizations under summertime midlatitude continental conditions, *Q. J. R. Meteorol. Soc.*, *128*(582), 1095–1135, doi:10.1256/003590002320373229.

Xie, S., R. T. Cederwall, and M. Zhang (2004), Developing long-term single-column model/cloud system–resolving model forcing data using numerical weather prediction products constrained by surface and top of the atmosphere observations, *J. Geophys. Res.*, *109*, D01104, doi:10.1029/2003JD004045.

Xie, S., et al. (2005), Simulations of midlatitude frontal clouds by single-column and cloud-resolving models during the Atmospheric Radiation Measurement March 2000 cloud intensive operational period, *J. Geophys. Res.*, *110*, D15S03, doi:10.1029/2004JD005119.

Xie, S., S. A. Klein, M. Zhang, J. J. Yio, R. T. Cederwall, and R. McCoy (2006), Developing large-scale forcing data for single-column and cloud-resolving models from the Mixed-Phase Arctic Cloud Experiment, *J. Geophys. Res.*, *111*, D19104, doi:10.1029/2005JD006950.

Xie, S., T. Hume, C. Jakob, S. A. Klein, R. B. McCoy, and M. Zhang (2010a), Observed large-scale structures and diabatic heating and drying profiles during TWP-ICE, *J. Clim.*, *23*(1), 57–79, doi:10.1175/2009jcli3071.1.

Xie, S., et al. (2010b), CLOUDS AND MORE: ARM climate modeling best estimate data, *Bull. Am. Meteorol. Soc.*, *91*(1), 13–20, doi:10.1175/2009BAMS2891.1.

Xie, S., Y. Zhang, S. E. Giangrande, M. P. Jensen, R. McCoy, and M. Zhang (2014), Interactions between cumulus convection and its environment as revealed by the MC3E sounding array, *J. Geophys. Res. Atmos.*, *119*, 11,784–11,808, doi:10.1002/2014JD022011.

Xu, K.-M., and A. Cheng (2013a), Evaluating low-cloud simulation from an upgraded multiscale modeling framework model. Part I: Sensitivity to spatial resolution and climatology, *J. Clim.*, *26*(16), 5717–5740, doi:10.1175/JCLI-D-12-00200.1.

Xu, K.-M., and A. Cheng (2013b), Evaluating low-cloud simulation from an upgraded multiscale modeling framework model. Part II: Seasonal variations over the eastern Pacific, *J. Clim.*, *26*(16), 5741–5760, doi:10.1175/JCLI-D-12-00276.1.

Xu, K.-M., and D. A. Randall (1996), Explicit simulation of cumulus ensembles with the GATE Phase III data: Comparison with observations, *J. Atmos. Sci.*, *53*(24), 3710–3736, doi:10.1175/1520-0469(1996)053<3710:ESOCEW>2.0.CO;2.

Xu, K.-M., et al. (2002), An intercomparison of cloud-resolving models with the Atmospheric Radiation Measurement summer 1997 Intensive Observation Period Data, *Q. J. R. Meteorol. Soc.*, *128*(580), 593–624, doi:10.1256/003590002321042117.

Xu, K.-M., et al. (2005), Modeling springtime shallow frontal clouds with cloud-resolving and single-column models, *J. Geophys. Res.*, *110* D15S04, doi:10.1029/2004JD005153.

Zhang, M., and J. Lin (1997), Constrained variational analysis of sounding data based on column-integrated budgets of mass, heat, moisture, and momentum: Approach and application to ARM measurements, *J. Atmos. Sci.*, *54*(11), 1503–1524, doi:10.1175/1520-0469(1997)054<1503:CVAOSD>2.0.CO;2.

Zhang, M., J. Lin, R. T. Cederwall, J. J. Yio, and S. C. Xie (2001), Objective analysis of ARM IOP Data: Method and sensitivity, *Mon. Weather Rev.*, *129*(2), 295–311, doi:10.1175/1520-0493(2001)129<0295:OAOAID>2.0.CO;2.

Zhang, M., et al. (2005), Comparing clouds and their seasonal variations in 10 atmospheric general circulation models with satellite measurements, *J. Geophys. Res.*, *110*, D15S02, doi:10.1029/2004JD005021.

Zhang, M., C. S. Bretherton, P. N. Blossey, S. Bony, F. Brient, and J.-C. Golaz (2012), The CGILS experimental design to investigate low cloud feedbacks in general circulation models by using single-column and large-eddy simulation models, *J. Adv. Model. Earth Syst.*, *4*, M12001, doi:10.1029/2012MS000182.

Zhao, C., et al. (2012), Toward understanding of differences in current cloud retrievals of ARM ground-based measurements, *J. Geophys. Res.*, *117*, D10206, doi:10.1029/2011JD016792.

Zhao, C., S. Xie, X. Chen, M. P. Jensen, and M. Dunn (2014), Quantifying uncertainties of cloud microphysical property retrievals with a perturbation method, *J. Geophys. Res. Atmos.*, *119*, 5375–5385, doi:10.1002/2013JD021112.